Synthesis, Characterization, and Electrochemistry of the Bis-Bridged Complexes $Me_2Si[\eta^5\text{-}C_5H_4Fe(CO)]_2[Ph_2P(CH_2)_nPPh_2]$ (n = 1–3) and $[Me_2Si[(\eta^5\text{-}C_5H_4)_2Fe_2(CO)_3]]_2[Ph_2P(CH_2)_nPPh_2]$ (n = 2, 3). Molecular Structures of $Me_2Si[\eta^5\text{-}C_5H_4Fe(CO)]_2[Ph_2P(CH_2)_nPPh_2]$ Where n = 1 and 3

Michael E. Wright, Thomas M. Mezza, Gregory O. Nelson,*[13] and Neal R. Armstrong*

Department of Chemistry, University of Arizona, Tucson, Arizona 85721

Victor W. Day and Michael R. Thompson

Department of Chemistry, University of Nebraska, Lincoln, Nebraska 68588

Received July 18, 1983

Photolysis of $Me_2Si[\eta^5\text{-}C_5H_4Fe(CO)_2]_2$ (1) with a series of bis(phosphines) (L = $Ph_2P(CH_2)_nPPh_2$, where n = 1, 2, and 3) leads to the formation of substituted dinuclear and tetranuclear compounds of the form $Me_2Si[\eta^5\text{-}C_5H_4Fe(CO)]_2[L]$ and $[Me_2Si[(\eta^5\text{-}C_5H_4)_2Fe_2(CO)_3]]_2[L]$, respectively. The ratio of these two types of compounds is dependent upon the ligand size (number of methylene units), stoichiometry, and the overall concentration employed. With the small ligands and dilute conditions, formation of the dinuclear product is favored. Under more concentrated reaction conditions and when an excess of 1 is used, the tetranuclear type of product becomes dominant. The electrochemistry of the dinuclear compounds indicate that *both* the silyl and the bis(phosphine) bridges are capable of stabilizing a two-electron oxidation product. This is demonstrated in the case of L = dppm where we observe, by fast-scan cyclic voltammetry, two, one-electron reversible oxidation steps. The structure of $Me_2Si[\eta^5\text{-}C_5H_4Fe(CO)]_2[dppm]$ (**3a**) is determined by X-ray diffraction. It crystallizes in the space group *Pnma* (No. 62) with a = 13.754 (4) Å, b = 17.707 (4) Å, c = 13.771 (3) Å and α, β, and γ = 90.00° with Z = 4. The structure was refined to R_1 = 0.041 and R_2 = 0.045 for 2226 independent reflections having $I > 3\sigma(I)$. The structure of $Me_2Si[\eta^5\text{-}C_5H_4Fe(CO)]_2[dppp]$ (**3c**) is also determined by X-ray diffraction. It crystallizes in the space group $P\bar{1}$ (No. 2) with a = 11.638 (11) Å, b = 11.833 (11) Å, c = 16.289 (14) Å, α = 111.22 (6)°, β = 72.67 (7)°, and γ = 107.02 (7)° with Z = 2. The structure is refined to R_1 = 0.067 and R_2 = 0.076 for 4115 independent reflections having $I > 3\sigma(I)$. The overall geometry of **3a** compared to **3c** implies that some distortion occurs from the steric requirements of the larger dppp ligand. This includes a significant lengthening of the Fe–Fe bond in complex **3c** by 0.024 (3) Å relative to **3a**.

Introduction

A variety of bridged metal–metal bonded transition-metal complexes are well documented in the literature.[1] These types of compounds are of interest since they allow a systematic approach to the study of the interactions between two metals. Two such systems previously reported are the cyclopentadienyl-bridged complex $Me_2Si[\eta^5\text{-}C_5H_4Fe(CO)_2]_2$ (1)[2] and a series of bis(phosphine)-bridged species $[\eta^5\text{-}C_5H_5Fe(CO)]_2[Ph_2P(CH_2)_nPPh_2]$ (where n = 1, 2, and 3).[3] In each system the bridge appears to be related to the observed chemistry and electrochemistry. For instance, 1 undergoes two one-electron electrochemical reduction steps, whereas the unbridged analogue has a single two-electron reduction step.[2] Futhermore, $[\eta^5\text{-}C_5H_5Fe(CO)]_2[dppe]$ exhibits stable multiple molecular oxidation states (0 and 1+), most likely arising by stabilization of the monocation by the bis(phosphine) bridge.[4] These experimental results suggest that the mechanical link can effectively stabilize weakly bonded metal–metal species.

We recently reported the preparation of some novel doubly linked binuclear and tetranuclear iron complexes.[5] These compounds utilize *both* a dicyclopentadienylsilyl link and a bridging bis(phosphine) ligand. The dinuclear compounds are especially intriguing because the two metals are held in close proximity, even when the bonding between the metals is destroyed. In addition, by varying the size of the bis(phosphine) ligand, one can systematically study the effects of changing the geometry in the complex. We report here full details on the synthesis and characterization of the dinuclear and tetranuclear compounds including two new derivatives. In the dinuclear series, molecular and crystal structures are determined for $Me_2Si[\eta^5\text{-}C_5H_4Fe(CO)]_2[dppm]$ (**3a**) and $Me_2Si[\eta^5\text{-}C_5H_4Fe(CO)]_2[dppp]$ (**3c**). Furthermore, the electrochemistry of the dinuclear complexes $Me_2Si[\eta^5\text{-}C_5H_4Fe(CO)]_2[L]$ (where L = dppm, dppe, and dppp) is reported and discussed.

Results and Discussion

Photolytic or thermally induced substitution of CO in $[\eta^5\text{-}C_5H_5Fe(CO)_2]_2$ by several bis(phosphine) ligands is known to lead to the bridged complexes $[\eta^5\text{-}C_5H_5Fe(CO)]_2[L]$ (where L = dppm, dppe, and dppp).[3] This reaction is thought to occur by a stepwise substitution of CO; however, the monosubstituted intermediates are never

(1) Poilblanc, R. *Inorg. Chim. Acta* **1982**, *62*, 75. Bergman, R. G. *Acc. Chem. Res.* **1980**, *13*, 113.
(2) Weaver, J.; Woodward, P. *J. Chem. Soc., Dalton Trans.* **1973**, 1439. Wegner, P. A.; Uski, V. A.; Kiester, R. P.; Dabestestani, S.; Day, V. W. *J. Am. Chem. Soc.* **1977**, *99*, 4846.
(3) Haines, R. J.; DuPreez, A. L. *J. Organomet. Chem.* **1970**, *21*, 181.
(4) Haines, R. J.; DuPreez, A. L. *Inorg. Chem.* **1972**, *12*, 330. Ferguson, J. A.; Meyer, T. J. *Inorg. Chem.* **1971**, *11*, 631.
(5) Nelson, G. O.; Wright, M. E. *J. Organomet. Chem.* **1980**, *206*, C21.

0276-7333/83/2302-1711$01.50/0

Scheme I

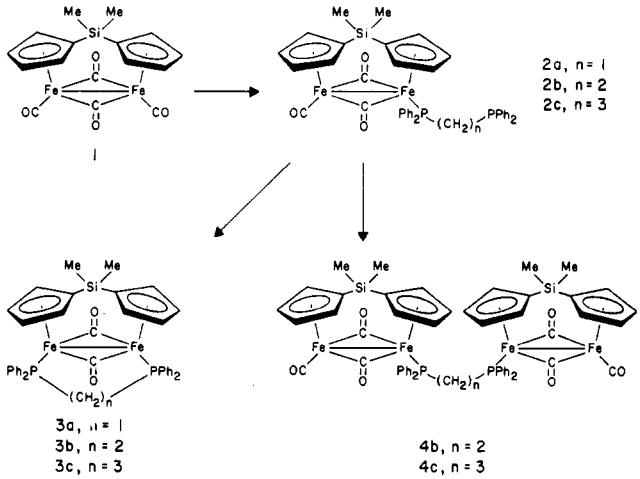

Table I. Summary of ^{1}H NMR Spectra for Complexes 3 and 4[a]

compd	C_5H_4	$SiCH_3$	$(CH_2)_n$	C_6H_5
3a	4.88 t[b] 4.58 m	0.42 s	1.78 t	7.3 m
3b	4.83 t[b] 4.27 m	0.40 s	1.37 d	7.3 m
3c	4.67 t[b] 4.22 m	0.40 s	1.2-1.8 m	7.3 m
4b	5.13 t, 4.87 t 4.63 t, 4.28 m	0.30 s	0.96 bs	7.4 m
4c	5.20 t, 4.91 t 4.67 bs, 4.20 m	0.35 s	1.6-1.9 m	7.3 m

[a] Spectra are recorded in $CDCl_3$, and the resonances are reported in ppm (δ) downfield from $(CH_3)_4Si$. Symbols used: s = singlet, d = doublet, t = triplet, m = multiplet, and b s = broad singlet. [b] An approximate coupling constant of 2 Hz is observed in these systems.

isolated. To prepare the bis-bridged compounds, we start with the cyclopentadienyl-bridged species $Me_2Si[\eta^5\text{-}C_5H_4Fe(CO)_2]_2$ (1). This complex is prepared in 20% yield by using a modified literature method.[6]

Irradiation of a benzene solution of 1 (~0.005 M) in the presence of the appropriate bis(phosphine) ligand results in the formation of both the di- and tetranuclear compounds 3 and 4, respectively (Scheme I). The photolysis mixtures are routinely washed with CH_3CN or acetone to remove the excess ligand and then subjected to column chromatography (alumina III). Elution with benzene typically gives two bands, an initial green band and a second, slower moving blue-green band. The green band is readily identified as the dinuclear complex 3 by its ^{1}H and ^{13}C NMR spectra (Tables I and II). The cyclopentadienyl (Cp) ring protons display two resonances in an AA'BB' pattern (complicated somewhat by coupling to the phosphorus) and three ^{13}C NMR resonances for the Cp ring carbons. The blue-green band, which is characterized as the tetranuclear species, has four ^{1}H NMR resonances and six ^{13}C NMR resonances for the Cp rings. This doubling in the number of NMR resonances is expected since there are clearly two types of Cp rings in the tetranuclear complexes 4.

A most intriguing aspect of the synthesis of these compounds is the dependence of the product distribution on the choice of ligand, stoichiometry of the reactants, and the concentration of the photolysis mixture employed. In each case the first step is substitution of CO by the bis(phosphine) ligand, thus giving the monodentate species

(6) Nelson, G. O.; Wright, M. E. *Ibid.* **1982**, *239*, 353.

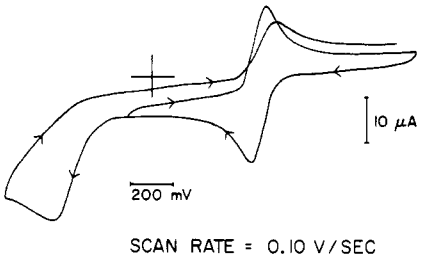

Figure 1. Voltammograms of **3a** in 0.02 M TBAP CH_2Cl_2 solution at 0.10 V/s scanning rate.

2.[7] Compound 2 can then undergo an intramolecular displacement of CO to yield 3 or react in an intermolecular fashion with a second molecule of 1 to give the tetranuclear species 4. Under the same reaction conditions (1/ligand, 1/1, mol/mol) but using different ligands, one can observe that dppm gives only trace amounts of **4a** while dppe and dppp yield increasing quantities of **4b** and **4c**, respectively, in that order. This trend can be related to the relative ease by which the bis(phosphine) can undergo the intramolecular CO substitution. As the number of methylene units increase, it appears more difficult for the ligand to fit into the required geometry of 3. This is certainly supported by examination of the molecular structures where **3c** shows significant distortion (see below). In a qualitative sense, the relative stabilities of these compounds, in solution, namely **3a > 3b > 3c**, are most likely due to the strain in the dinuclear system; where in the case of **3c**, the strain becomes an overwhelming factor. It is not surprising to find that under conditions of excess ligand (3-fold) that the major product isolated in the case of all three bis(phosphines) is 3. Presumably once complex 2 is formed, using all of 1, only an intramolecular type of reaction is likely. On the other hand, higher concentrations for the photolysis solutions and a stoichiometry of 2/1 for 1/ligand favor the intermolecular type reaction, thus, giving a larger proportion of the tetranuclear species.

Another aspect of the ^{1}H NMR worth noting is the relative upfield shift in the methylene resonances of **3b** and **4b** relative to the free ligand. The upfield shift is indicative of a shielding effect by a nearby ring current or σ donation of electron density into the ligand. As earlier studies have pointed out, electron density is withdrawn from the phosphine ligand by complexation to the metal, and therefore, an inductive type of electron donation is unlikely.[8] In the related bis(phosphine) compounds $[(\eta^5\text{-}C_5H_4)Fe(CO)]_2[Ph_2P(CH_2)_nPPh_2]$ (n = 1–3) Haines and DuPreez also observed a similar upfield shift of the methylene proton resonances.[3] They attribute this shift to the shielding effect of a ring current in the Fe–CO plane, which the methylene protons are positioned directly below. This effect certainly appears to be present in both 3 and 4; however, at first it is not so clear why the methylene protons of 4 are farther upfield than those of 3. From examination of models it appears that indeed complex 4's methylene protons can approach the Fe–CO plane as close as those of 3. We suggest in addition to the latter effect that upfield shift of the methylene resonances in the tetranuclear and possibly the dinuclear compounds is in part due to the shielding effects of the phenyl rings on the

(7) The monosubstituted complexes $Me_2Si[(C_5H_4)_2Fe_2(CO)_3][L]$ (L = dppm and dppe) have been isolated as stable crystalline products. It is noteworthy to mention that they become the major product when the photolysis lamp (medium-pressure Hg) drops in intensity due to extended use (1000 h). Details on these compounds will be published elsewhere; G. O. Nelson and M. E. Wright.

(8) King, R. B.; Eggers, C. A. *Inorg. Chem. Acta* **1968**, *2*, 33. Haines, R. J.; Nyholm, R. S.; Stiddard, M. H. B. *J. Chem. Soc. A* **1967**, 94.

Table II. Summary of ^{13}C NMR Spectra for Complexes 3 and 4[a]

compd	C_5H_4	$SiCH_3$	$(CH_2)_n$	C_6H_5	CO
3a	78.13, 86.65, 98.22	−2.68	28.33	127.80-136.90	298.29 t
3b	82.80, 88.07, 95.33	−2.91	23.17 d, J = 29.3 Hz	127.96-137.75	296.38 t
3c	94.28, 89.73, 84.30	−2.67	26.06 t, J = 13.2 Hz 18.88	127.81-139.99	300.35 t
4b	82.87, 86.23, 88.11, 89.99, 94.8, 96.22	−3.22	23.07	128.01-133.62	216.08 282.59 t
4c	82.61, 86.23,[b] 89.85, 95.02, 96.31	−3.17	30.16 m 19.46	127.92-135.09	216.47 282.76 t

[a] Spectra are recorded in $CDCl_3$ and resonances are reported in ppm (δ) downfield from $(CH_3)_4Si$. All resonances can be assumed to be singlets unless otherwise specified. Symbols used: d = doublet and t = triplet. [b] One silyl bound C_5H_4 carbon resonance is located at 89.85 ppm determined through partial proton-coupled spectra.

Table III. Cyclic Voltammetry of the Dinuclear Complexes $Me_2Si[\eta^5\text{-}C_5H_4Fe(CO)]_2[Ph_2P(CH_2)_nPPh_2]$ (Where n = 1, 2, and 3)[a]

compd	scan rate, V/s	first oxidation, V			second oxidation, V		
		E_{p_a}	E_{p_c}	ΔE_p	E_{p_a}	E_{p_c}	ΔE_p
ferrocene	0.10	+0.10	+0.03	0.07			
3a	0.10	−0.28	−0.36	0.08	+0.57		
	10	−0.24	−0.41	0.17	+0.59	+0.46	0.13
3b	0.10	−0.36	−0.44	0.08	+0.48		
	10	−0.32	−0.49	0.17	+0.55		
3c	0.10	−0.42	−0.49	0.07	+0.50		
	10	−0.32	−0.52	0.20	+0.58		
$[C_5H_5Fe(CO)]_2$[dppm]	0.10	−0.35	−0.42	0.07	+0.48		
	10	−0.30	−0.46	0.16	+0.60		
$[C_5H_5Fe(CO)]_2$[dppe]	0.10	−0.39	−0.46	0.07	+0.36		

[a] Voltammograms are recorded in 0.2 M TBAP CH_2Cl_2 solutions.

ligand. Examination of the crystal and molecular structures of **3a** and **3c** reveal that the phenyl moieties are in a geometry to cause such an effect.

Electrochemistry

The cyclic voltammograms of compound **3a** in 0.2 M tetrabutylammonium perchlorate (TBAP) dichloromethane solution are shown in Figure 1 at a scan rate of 0.10 V/s. All three compounds show very similar electrochemical behavior with current peaks corresponding to the removal of two electrons via one-electron transfers.

The anodic and cathodic peak voltages, E_{p_a} and E_{p_c}, respectively, are listed in Table III for **3** and selected reference compounds along with the potential difference between the peaks of ΔE_p. All three dinuclear compounds show a chemically reversible one-electron oxidation as determined by thin-layer coulometry. Increasing the length of the bridging chain between the phosphine groups from methyl, ethyl, to trimethylene causes a negative shift of the first oxidation potentials indicating that the ease of electron removal is **3c > 3b > 3a**. Interestingly, the UV–vis spectra (Table IV) of complexes **3** show a decrease in the energy for the visible band which coincides with the relative ease of electron removal from the highest occupied molecular orbital (HOMO). Furthermore, the molecular structures of **3a** and **3c** clearly define a lengthening (0.024 Å) of the M–M distance in **3c** relative to **3a**, which could indicate a destabilization of the molecular orbitals responsible for retaining the two metals "bonded". A recent study on the related system $[\eta^5\text{-}C_5H_5Fe(CO)]_2[L]$ (L = dppm and dppe) by Hall[9] indicates the HOMO *not* to be the Fe–Fe σ bond but is rather an orbital consisting largely of Fe–CO and Fe–P bonding. Our data are consistent with the idea that the sterically crowded phosphine ligand (dppp and to a lesser extent dppe) are increasing the distance between the two metal centers which is in turn effecting the Fe–CO bonding. It also is reasonable to

(9) Sherwood, D. E.; Hall, M. B. *Inorg. Chem.* **1978**, *17*, 3397.

Table IV. Summary of UV-vis Data for Complexes 3a-c[a]

complex	λ_{max} (ϵ), nm (L/mol cm)
3a	616 (4.3×10^2), 385 (3.9×10^3), 232 (4.3×10^4)
3b	648 (4.0×10^2), 385 (3.8×10^3), 232 (3.2×10^4)
3c	682 (4.3×10^2), 389 (4.2×10^3), 231 (4.1×10^4)

[a] Spectra are recorded in CH_2Cl_2.

suggest that the increase in the P–Fe–Fe–P torsion angle from **3a** (0.0°) (The torsion angle of 0.0° is implied by the crystallographic mirror plane imposed in **3a**.) to **3c** (13.6°) is connotative of a decrease in orbital overlap, therefore, weakening the Fe–P bond in **3c** relative to **3a**. The comparative ease for removal of an electron, the shift in the visible light absorption, and the lengthening of the metal–metal distance are all consistent with an increase in energy for the HOMO of **3c** relative to **3a**.

At a scan rate of 0.10 V/s, the second oxidation for all three compounds is chemically irreversible forming decomposition products that coat the electrode surface. This process is illustrated in the voltammograms in Figure 1 where the first two scans are shown for **3a**. The first scan is reversed after the initial oxidation event, and its chemical reversibility is demonstrated. However, if the potential is scanned past the second oxidation peak, very little or no reduction current is observed. In addition, the peak current for the reduction of the first chemically reversible oxidation is reduced and the wave is broadened. Successive voltammograms for the first oxidation peak only are broadened, and the peak currents are reduced which is typical of an absorbed product partially blocking the electrode surface and restricting the charge-transfer kinetics. This effect is most striking for compound **3c**, less pronounced for **3b**, and **3a**, in that order. This voltammetric behavior suggests that the stabilities of the dications resulting from the two successive oxidations are **3a > 3b > 3c**.

This stability order can be further tested by using fast-scan cyclic voltammetry. The two-electron oxidation

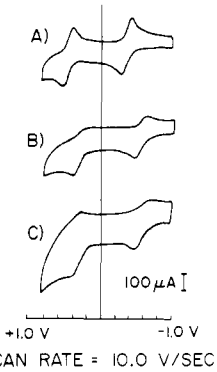

Figure 2. Fast scan voltammograms in 0.02 M TBAP CH_2Cl_2 solutions at a scanning rate of 10.0 V/s for (A) **3a**, (B) **3b**, and (C) **3c**.

products probably follow an EC mechanism where the dication undergoes an irreversible first-order decomposition reaction. It is possible to increase the observed chemical reversibility of the dications by increasing the potential scan rate. When the scan rate is increased, the time elapsed between the formation of the dication and its reduction back to the more stable monocation is decreased. It should be possible to increase the scan rate to the point where the dication is reduced back to the monocation before it has a chance to decompose and therefore determine a rate constant for the decomposition reaction. The smaller this rate constant, the more stable the dication. The fast scan voltammograms for compounds **3a**, **3b**, and **3c** are shown in Figure 2 at 10.0 V/s. At this scan rate, two one-electron chemically reversible oxidations are seen for compound **3a**. The second oxidation remains irreversible for compounds **3b** and **3c** up to scan rates of 100 V/s. Using the method of Nicholson,[10] we are able to estimate the rate constant for the decomposition of the dication $[\mathbf{3a}]^{2+}$ from the change in the ratio of the cathodic and anodic peak current ($i_{p,c}/i_{p,a}$) with the scan rate. We calculate an average first-order constant, k_f, for the decomposition reaction of $[\mathbf{3a}]^{2+}$ to be 3.1 ± 0.5 s^{-1}.

$$[\mathbf{3a}]^{+} \rightleftarrows [\mathbf{3a}]^{2+}$$

$$[\mathbf{3a}]^{2+} \xrightarrow{k_f} \text{decomposition products}$$

To access the contribution of the silyl bridge in these systems, we studied the $[C_5H_5Fe(CO)]_2$[dppm] system by using fast-scan cyclic voltammetry. As expected, it is found that the latter complex does not display a reversible second oxidation step but an event which is only partially reversible. Therefore, it is reasonable to conclude that the silyl bridge does aid in stabilizing the dicationic species $[\mathbf{3a}]^{2+}$.

Crystal and Molecular Structures of $Me_2Si[\eta^5\text{-}C_5H_4Fe(CO)]_2$[L] Where L = dppm (3a) and dppp (3c)

Crystals of **3a** are obtained by slow evaporation of a CH_2Cl_2–CH_3CN (1/1, v/v) solution containing the complex. In an analogous manner X-ray quality crystals of **3c** are secured by the use of a CH_2Cl_2–CH_3NO_2 (1/1, v/v) solution. Perspective ORTEP views for **3a** showing the labeling scheme employed are presented in Figure 3. Selected bond lengths and angles are listed in Tables X and XII, respectively. In Figure 4 a perspective ORTEP view of **3c** is depicted along with the atom labeling scheme. Selected bond lengths and angles for complex **3c** are set out in Tables XI and XIII, respectively.

(10) Nicholson, R. S.; Shain, I. *Anal. Chem.* **1964**, *36*, 706.

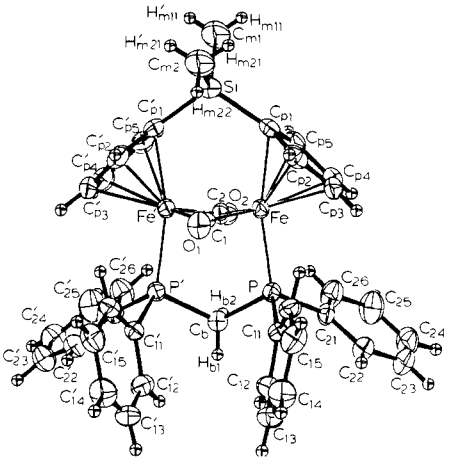

Figure 3. Perspective ORTEP drawing of $Me_2Si[\eta^5\text{-}C_5H_4Fe(CO)]_2$[dppm] (**3a**) with non-hydrogen atoms represented by thermal vibration ellipsoids drawn to encompass 50% of the electron density. Hydrogen atoms are represented by arbitrarily small spheres for clarity.

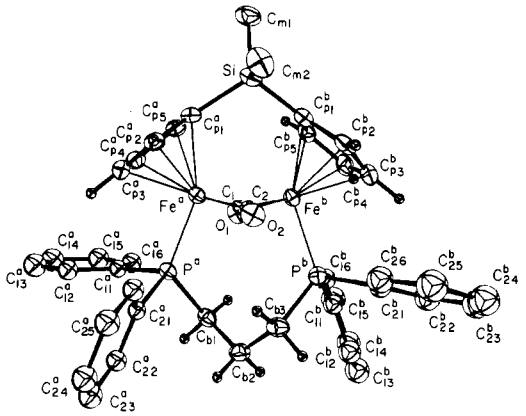

Figure 4. Perspective ORTEP drawing of $Me_2Si[\eta^5\text{-}C_5H_4Fe(CO)]_2$[dppp] (**3c**) with non-hydrogen atoms represented by thermal vibration ellipsoids and group atoms represented by thermal spheres to encompass 30% of the electron density. Selected hydrogen atoms are represented by arbitrarily small spheres for clarity.

Comparison of the two molecular structures for **3a** and **3c** display interesting differences which seem to be the result of increasing the steric bulk in the bis(phosphine) link. Of particular interest is the 0.024 Å lengthening of the metal–metal distance in **3c** relative to **3a**. This increase in distance between the metals is likely sterically induced by increasing the number of methylene units in the bis(phosphine) ligand from 1 in **3a** to 3 in **3c**. Our spectroscopic and electrochemical data (see above) indicate that as the dinuclear species **3c** undergoes distortion and accommodates the steric demands of the phosphine ligand the Fe–P and Fe–CO bonding in the system is destabilized. Related to the lengthing of the metal–metal distance is the opening of the C_p–Si–C_p and Fe–Fe–P bond angles in **3c** (111.5° and 108.8°) relative to **3a** (109.4° and 97.3°). The remaining bond angles and lengths are similar for **3a** and **3c**, and these resemble the tetracarbonyl analogue $Me_2Si[\eta^5\text{-}C_5H_4Fe(CO)_2]_2$. We feel that the differences between the geometrical parameters for **3a** and **3c** are indicative of the strain imposed by the dppp ligand into the idealized geometry of these dinuclear systems.[11] It

(11) The $Me_2Si[C_5H_4Fe(CO)_2]_2$ (**1**) complex is assumed to possess a minimum of steric interactions between the terminal carbonyls and is utilized as the model system. See ref 2 for details concerning the geometric parameters of **1**.

Table V. Crystallographic Parameters

parameter	3a	3c
space group	*Pnma*	$P\bar{1}$
a, Å	13.754 (4)	11.638 (11)
b, Å	17.707 (4)	11.833 (11)
c, Å	13.771 (3)	16.289 (14)
α, deg	90.00	111.22 (6)
β, deg	90.00	72.76 (7)
γ, deg	90.00	107.02 (7)
V, Å^3	3354 (3)	1953 (3)
d_{calcd}, g/cm^3	1.46	1.30
Z	4	2
fw	738.45	766.50
cryst size, mm	0.38 × 0.38 × 0.50	0.23 × 0.33 × 0.17
μ(Mo K$\bar{\alpha}$), cm^{-1}	10.3	8.85
scan method	ω	$2\theta:\theta$
range 2θ, deg	0-55.0	4.0-50.0
no. of unique data	3964	6924
no. of data with $\lvert F_o^2\rvert > 3\sigma\lvert F_o^2\rvert$	2226	4115
R_1	0.041	0.067
R_2	0.045	0.076
no. of variables	296	320
goodness of fit	1.3	2.4

Table VI. Atomic Coordinates for Non-Hydrogen Atoms in Crystalline $Me_2Si[\eta^5\text{-}C_5H_4Fe(CO)]_2$[dppm][a]

atom type[b]	fractional coordinates		
	0.18181 (4)	0.32052 (3)	0.05928 (4)
P	0.03726 (7)	0.33623 (5)	0.12195 (8)
Si	0.3797 (1)	0.2500[c]	−0.0608 (2)
O_1	0.0909 (3)	0.2500[c]	−0.1087 (3)
O_2	0.2344 (3)	0.2500[c]	0.2425 (3)
C_1	0.1267 (4)	0.2500[c]	0.308 (4)
C_2	0.2068 (4)	0.2500[c]	0.1598 (5)
C_{p_1}	0.3165 (3)	0.3364 (2)	−0.0137 (3)
C_{p_2}	0.2418 (3)	0.3800 (2)	−0.0593 (4)
C_{p_3}	0.2040 (3)	0.4314 (2)	0.0068 (4)
C_{p_4}	0.2536 (3)	0.4223 (3)	0.0960 (4)
C_{p_5}	0.3233 (3)	0.3649 (2)	0.0826 (4)
C_{11}	−0.0659 (3)	0.3549 (2)	0.0413 (3)
C_{12}	−0.1618 (3)	0.3422 (3)	0.0712 (4)
C_{13}	−0.2370 (3)	0.3521 (3)	0.0059 (4)
C_{14}	−0.2198 (4)	0.3767 (3)	−0.0863 (4)
C_{15}	−0.1267 (4)	0.3925 (3)	−0.1155 (4)
C_{16}	−0.0494 (3)	0.3802 (2)	−0.0518 (3)
C_{21}	−0.0242 (3)	0.4095 (2)	0.2157 (3)
C_{22}	0.0451 (3)	0.4667 (3)	0.2105 (4)
C_{23}	−0.0487 (4)	0.5225 (3)	0.2808 (4)
C_{24}	0.0144 (4)	0.5221 (3)	0.3573 (4)
C_{25}	0.0840 (5)	0.4666 (3)	0.3630 (4)
C_{26}	0.0888 (4)	0.4106 (3)	0.2928 (4)
C_{m_1}	0.5073 (6)	0.2500[c]	−0.0146 (9)
C_{m_2}	0.3749 (11)	0.2500[c]	−0.1943 (8)
C_b	−0.0005 (4)	0.2500[c]	0.1873 (4)

[a] The numbers in parentheses are the estimated standard deviations in the last significant digit. [b] Atoms are labeled in agreement with Figure 3. [c] This is a symmetry-required value and is therefore listed without an estimated standard deviation.

is clear from the contrasts in the molecular structures for **3a** and **3c** that the overall geometry of linked dinuclear complexes is quite sensitive to ligand changes, specifically, in the present system the number of methylene units in the bis(phosphine) bridge.

Summary

By irradiation of **1** in the presence of various bis(phosphines) we are able to prepare a new class of bis-bridged dinuclear and tetranuclear iron complexes. The reaction conditions employed can be controlled in such a manner as to enable either the dinuclear or tetranuclear species to be isolated as the major product. In addition, the three bis(phosphines) utilized are found to change the structures

Table VII. Atomic Coordinates for Non-Hydrogen and Nongroup Atoms in Crystalline $Me_2Si[\eta^5\text{-}C_5H_4Fe(CO)]_2$[dppp][a]

atom type[b]	fractional coordinates		
	x	*y*	*z*
Fe^a	0.81183 (9)	0.53398 (10)	0.71568 (7)
Fe^b	0.76069 (10)	0.65448 (10)	0.63619 (7)
P^a	0.9039 (2)	0.6633 (2)	0.8246 (1)
P^b	0.7823 (2)	0.8482 (2)	0.7192 (1)
Si	0.6222 (2)	0.3478 (2)	0.5684 (1)
C_1	0.9138 (7)	0.6313 (7)	0.6395 (4)
O_1	1.0202 (5)	0.6538 (5)	0.6041 (3)
C_2	0.6744 (7)	0.6073 (7)	0.7433 (5)
O_2	0.5759 (5)	0.6066 (5)	0.7931 (3)
$C_{p_1}{}^a$	0.7238 (7)	0.3577 (7)	0.6415 (5)
$C_{p_2}{}^a$	0.6942 (7)	0.3668 (7)	0.7347 (5)
$C_{p_3}{}^a$	0.8012 (8)	0.3883 (7)	0.7643 (5)
$C_{p_4}{}^a$	0.9030 (7)	0.3912 (7)	0.6885 (6)
$C_{p_5}{}^a$	0.8553 (7)	0.3715 (7)	0.6143 (5)
$C_{p_1}{}^b$	0.6699 (7)	0.4965 (7)	0.5441 (5)
$C_{p_2}{}^b$	0.6046 (7)	0.5936 (9)	0.5750 (5)
$C_{p_3}{}^b$	0.6836 (9)	0.6973 (8)	0.5506 (6)
$C_{p_4}{}^b$	0.7975 (8)	0.6669 (8)	0.5020 (5)
$C_{p_5}{}^b$	0.7891 (7)	0.5459 (8)	0.4936 (5)
C_{m_1}	0.6469 (9)	0.2202 (9)	0.4609 (6)
C_{m_2}	0.4567 (7)	0.3248 (9)	0.6312 (6)
C_{b_1}	0.9772 (7)	0.8233 (7)	0.8248 (5)
C_{b_2}	0.8967 (8)	0.9173 (7)	0.8716 (5)
C_{b_3}	0.7743 (7)	0.8880 (7)	0.8417 (5)
S_1	0.246 (2)	0.824 (2)	−0.016 (2)
S_2	0.228 (4)	0.763 (2)	0.042 (1)
S_3	0.476 (2)	0.857 (3)	0.029 (2)
S_4	0.378 (3)	0.774 (4)	0.073 (2)
S_5	0.652	0.198	0.028
S_6	0.610 (6)	0.243 (5)	0.006 (3)

[a] The numbers in parentheses are the estimated standard deviations in the last significant digit. [b] Atoms are labeled in agreement with Figure 4.

of dinuclear species, resulting in noticeable deviations in their UV spectra and electrochemistry. From the electrochemistry it is evident that both dppm and the silyl bridge have the ability to maintain the geometry of the dinuclear system upon a decrease of bonding forces between the metals to a much higher degree than dppe and especially dppp. Finally, this study illustrates how small changes in structural design can alter the molecular framework and consequently the properties of the dinuclear complexes. Further studies on the chemical reactivity of these systems are currently underway in our laboratory.

Experimental Section

General Data. All manipulation of complexes and solvents are carried out by using standard Schlenck techniques. Solvents are degassed and purified by distillation under nitrogen from standard drying agents.[12] Spectroscopic measurements utilize the following instrumentation: ^{1}H NMR, Varian EM 360, Bruker 250 FT (at 250 MHz); ^{13}C NMR, Bruker 250 FT (at 62.9 MHz); ^{31}P NMR, Bruker 250 FT (at 101.3 MHz); IR, Perkin-Elmer 398; UV, Perkin-Elmer 552. The NMR chemical shifts are reported in δ vs. Me_4Si assigning the $CDCl_3$ resonance in ^{13}C spectra to be at 77.00 ppm and in ^{31}P spectra an external reference of H_3PO_4 is assigned 0.00 ppm. Carbon-13 spectra are run with ^{1}H decoupling, and resonances may be assumed to be singlets unless multiplicity is specified. The $Me_2Si[\eta^5\text{-}C_5H_4Fe(CO)_2]_2$ is prepared by a recent modification of a previously reported method. The bis(diphenylphosphino)methane (dppm), 1,2-bis(diphenylphosphino)ethane (dppe), and 1,3-bis(diphenylphosphino)propane (dppp) are purchased from Strem Chemicals and used as received. Irradiations are conducted by using a Hanovia photochemical

(12) Gordon, A. J.; Ford, R. A. "The Chemists Companion"; Wiley: New York, 1972.

Table VIII. Atomic Coordinates for Hydrogen Atoms in Crystalline $Me_2Si[\eta^5\text{-}C_5H_4Fe(CO)]_2$[dppm][a]

atom type[b]	fractional coordinates			B,[d] Å^2
	x	y	z	
H_{p_2}	0.225 (3)	0.376 (2)	0.118 (3)	2 (1)
H_{p_3}	0.157 (3)	0.467 (3)	−0.004 (3)	4 (1)
H_{p_4}	0.247 (4)	0.447 (3)	0.156 (3)	4 (1)
H_{p_5}	0.363 (3)	0.350 (2)	0.132 (3)	3 (1)
H_{12}	−0.174 (4)	0.324 (3)	0.135 (3)	4 (1)
H_{13}	−0.294 (3)	0.341 (2)	0.024 (3)	3 (1)
H_{14}	−0.267 (3)	0.380 (3)	−0.136 (3)	4 (1)
H_{15}	−0.117 (3)	0.407 (2)	−0.177 (3)	3 (1)
H_{16}	0.012 (3)	0.393 (2)	−0.074 (3)	2 (1)
H_{22}	−0.089 (3)	0.468 (3)	0.160 (3)	3 (1)
H_{23}	−0.096 (3)	0.560 (3)	0.276 (4)	4 (1)
H_{24}	0.013 (3)	0.562 (3)	0.404 (3)	4 (1)
H_{25}	0.128 (4)	0.468 (3)	0.416 (4)	7 (2)
H_{26}	0.139 (3)	0.374 (3)	0.298 (3)	4 (1)
H_{m11}	0.537 (4)	0.289 (3)	−0.029 (4)	8 (2)
H_{m12}	0.513 (8)	0.250[c]	0.062 (8)	10 (3)
H_{m21}	0.398 (4)	0.289 (3)	−0.216 (4)	8 (2)
H_{m22}	0.298 (12)	0.250[c]	−0.220 (12)	21 (6)
H_{b1}	−0.062 (4)	0.250[c]	0.205 (4)	2 (1)
H_{b2}	0.033 (4)	0.250[c]	0.248 (4)	2 (1)

[a] The numbers in parentheses are the estimated standard deviations in the last significant digit. [b] Atoms are labeled in agreement with Figure 3. [c] This is a symmetry-required value and is therefore listed without an estimated standard deviation. [d] Isotropic thermal parameter.

Table IX. Atomic Coordinates for Group Atoms in Crystalline $Me_2Si[\eta^5\text{-}C_5H_4Fe(CO)]_2$[dppp][a]

atom type[b]	fractional coordinates			B,[c] Å^2
	x	y	z	
$C_{11}{}^a$	1.2430 (5)	0.5250 (6)	0.8111 (4)	6.1 (2)
$C_{12}{}^a$	1.1366 (6)	0.5038 (5)	0.8746 (4)	5.7 (2)
$C_{13}{}^a$	1.0351 (4)	0.5470 (5)	0.8807 (3)	4.1 (2)
$C_{14}{}^a$	1.0400 (4)	0.6113 (5)	0.8233 (4)	3.2 (1)
$C_{15}{}^a$	1.1464 (5)	0.6324 (5)	0.7598 (3)	4.4 (2)
$C_{16}{}^a$	1.2480 (4)	0.5892 (6)	0.7537 (4)	5.4 (2)
$C_{21}{}^a$	0.8099 (5)	0.7791 (5)	1.1016 (3)	4.6 (2)
$C_{22}{}^a$	0.8749 (3)	0.7625 (5)	1.0134 (3)	3.8 (2)
$C_{23}{}^a$	0.8193 (4)	0.6830 (5)	0.9433 (2)	3.0 (1)
$C_{24}{}^a$	0.6986 (4)	0.6202 (4)	0.9613 (3)	3.9 (2)
$C_{25}{}^a$	0.6336 (4)	0.6368 (5)	1.0495 (4)	4.8 (2)
$C_{26}{}^a$	0.6893 (5)	0.7162 (5)	1.1197 (3)	4.8 (2)
$C_{11}{}^b$	1.1273 (5)	1.1335 (6)	0.6410 (5)	7.0 (3)
$C_{12}{}^b$	1.0355 (7)	1.1716 (4)	0.7146 (5)	7.0 (3)
$C_{13}{}^b$	0.9310 (5)	1.0865 (6)	0.7369 (4)	5.5 (2)
$C_{14}{}^b$	0.9183 (5)	0.9631 (5)	0.6857 (4)	4.1 (2)
$C_{15}{}^b$	1.0101 (6)	0.9250 (5)	0.6121 (4)	5.2 (2)
$C_{16}{}^b$	1.1146 (5)	1.0101 (7)	0.5898 (4)	7.4 (3)
$C_{21}{}^b$	0.4499 (5)	1.0007 (7)	0.7376 (5)	7.1 (3)
$C_{22}{}^b$	0.5644 (7)	1.0472 (6)	0.6919 (5)	6.9 (3)
$C_{23}{}^b$	0.6659 (5)	1.0044 (6)	0.6862 (4)	5.9 (2)
$C_{24}{}^b$	0.6529 (5)	0.9150 (6)	0.7261 (4)	4.4 (2)
$C_{25}{}^b$	0.5384 (6)	0.8684 (5)	0.7718 (4)	5.7 (2)
$C_{26}{}^b$	0.4369 (5)	0.9112 (7)	0.7776 (5)	7.6 (3)

[a] The numbers in parentheses are the estimated standard deviations in the last significant digit. [b] Atoms are labeled in agreement with Figure 4. [c] Isotropic thermal parameter.

reactor utilizing a 450-W medium-pressure mercury lamp as the light source unless otherwise noted. All of the electrochemical studies are performed in dichloromethane solution with 0.2 M tetrabutylammonium perchlorate (TBAP) as the supporting electrolyte. The dichloromethane (Burdich and Jackson, Muskegon, MI) is dried over activated neutral alumina (Alpha Products, Danvers, MA) before use. TBAP (Eastman Kodak) is recrystallized twice from an ethyl acetate–pentane mixture and dried under vacuum at 80 °C.

Electrochemical Measurements. A cell employing a three-electrode configuration is used in the electrochemical studies.

Table X. Bond Lengths (Å) Involving Non-Hydrogen Atoms in Crystalline $Me_2Si[\eta^5\text{-}C_5H_4Fe(CO)]_2$[dppm][a,b]

Fe–Fe′[c]	2.497 (1)	C_1–O_1	1.181 (7)
		C_2–O_2	1.200 (8)
Fe–P	2.185 (1)		
		C_{p_1}–C_{p_2}	1.430 (6)
Fe–C_1	1.916 (4)	C_{p_1}–C_{p_5}	1.422 (7)
Fe–C_2	1.896 (4)	C_{p_2}–C_{p_3}	1.389 (7)
		C_{p_3}–C_{p_4}	1.414 (7)
Fe–C_{p_1}	2.127 (4)	C_{p_4}–C_{p_5}	1.409 (6)
Fe–C_{p_2}	2.111 (5)		
Fe–C_{p_3}	2.114 (4)	C_{11}–C_{12}	1.400 (6)
Fe–C_{p_4}	2.117 (5)	C_{11}–C_{16}	1.377 (6)
Fe–C_{p_5}	2.123 (5)	C_{12}–C_{13}	1.381 (7)
		C_{13}–C_{14}	1.364 (8)
Fe–C_g[d]	1.795 (–)	C_{14}–C_{15}	1.372 (7)
		C_{15}–C_{16}	1.395 (7)
P–C_{11}	1.832 (4)	C_{21}–C_{22}	1.393 (6)
P–C_{21}	1.839 (4)	C_{21}–C_{26}	1.385 (7)
		C_{22}–C_{23}	1.385 (7)
P–C_b	1.847 (3)	C_{23}–C_{24}	1.365 (8)
		C_{24}–C_{25}	1.375 (8)
Si–C_{p_1}	1.875 (4)	C_{25}–C_{26}	1.386 (8)
Si–C_{m_1}	1.867 (9)		
Si–C_{m_2}	1.839 (11)		

[a] The numbers in parentheses are the estimated standard deviations in the last significant digit. [b] Atoms are labeled in agreement with Figure 3. [c] Primed (′) atoms are related to nonprimed atoms by the crystallographic mirror plane at $y = 1/4$. [d] The symbol C_g is used to denote the center of gravity for the 5-membered ring whose atoms carry subscripted p's.

Table XI. Bond Lengths Involving Non-Hydrogen Atoms in Crystalline $Me_2Si[\eta^5\text{-}C_5H_4Fe(CO)]_2$[dppp][a,b]

Fe^a–Fe^b	2.521 (3)		
Fe^a–P^a	2.200 (3)	Fe^b–P^b	2.183 (3)
Fe^a–C_1	1.908 (8)	Fe^b–C_1	1.899 (9)
Fe^a–C_2	1.902 (9)	Fe^b–C_2	1.924 (8)
Fe^a–$C_{p_1}{}^a$	2.126 (7)	Fe^b–$C_{p_1}{}^b$	2.148 (7)
Fe^a–$C_{p_2}{}^a$	2.119 (8)	Fe^b–$C_{p_2}{}^b$	2.145 (9)
Fe^a–$C_{p_3}{}^a$	2.102 (10)	Fe^b–$C_{p_3}{}^b$	2.126 (13)
Fe^a–$C_{p_4}{}^a$	2.099 (10)	Fe^b–$C_{p_4}{}^b$	2.150 (9)
Fe^a–$C_{p_5}{}^a$	2.111 (7)	Fe^b–$C_{p_5}{}^b$	2.123 (7)
Fe^a–$C_g{}^a$[c]	1.734 (–)	Fe^b–$C_g{}^b$[c]	1.770 (–)
P^a–$C_{11}{}^a$	1.852 (7)	P^b–$C_{11}{}^b$	1.848 (6)
P^a–$C_{21}{}^a$	1.855 (4)	P^b–$C_{21}{}^b$	1.854 (8)
P^a–$C_{b_1}{}^a$	1.834 (9)	P^b–$C_{b_3}{}^b$	1.858 (9)
Si–$C_{p_1}{}^a$	1.866 (10)	Si–$C_{p_1}{}^b$	1.834 (9)
Si–C_{m_1}	1.863 (9)		
Si–C_{m_2}	1.886 (8)		
$C_{p_1}{}^a$–$C_{p_2}{}^a$	1.424 (12)	$C_{p_1}{}^b$–$C_{p_2}{}^b$	1.421 (14)
$C_{p_2}{}^a$–$C_{p_3}{}^a$	1.389 (14)	$C_{p_2}{}^b$–$C_{p_3}{}^b$	1.408 (13)
$C_{p_3}{}^a$–$C_{p_4}{}^a$	1.438 (11)	$C_{p_3}{}^b$–$C_{p_4}{}^b$	1.402 (13)
$C_{p_4}{}^a$–$C_{p_5}{}^a$	1.394 (14)	$C_{p_4}{}^b$–$C_{p_5}{}^b$	1.388 (14)
$C_{p_5}{}^a$–$C_{p_1}{}^a$	1.438 (11)	$C_{p_5}{}^b$–$C_{p_1}{}^b$	1.430 (10)
C_{b_1}–C_{b_2}	1.507 (12)	C_{b_2}–C_{b_3}	1.544 (13)

[a] The numbers in parentheses are the estimated standard deviations in the last significant digit. [b] Atoms are labeled in agreement with Figure 4. [c] The symbols $C_g{}^a$ and $C_g{}^b$ are used to denote the center of gravity for the 5-membered rings whose atoms carry subscripted p's.

A platinum wire with a geometric area of 0.2 cm^2 is used as the working electrode and coiled platinum wire serves as the counter electrode. All potentials are reported vs. an aqueous silver–silver perchlorate reference electrode that is separated from the bulk solution by a ceramic frit and a salt bridge containing 0.2 M TBAP in dichloromethane. The stability of this reference electrode, 5 mV, is checked by measuring the peak potentials of the ferrocene–ferrocenium ion couple after the current–voltage measurements for each compound are completed. Each of the solutions are deoxygenated by at least two consecutive freeze–pump–thaw cycles prior to use.

A potentiostat of conventional operation amplifier design with a positive feedback circuit for IR compensation is used for all current–voltage measurements. Cyclic voltammograms are re-

Table XII. Bonds Angles (deg) Involving Non-Hydrogen Atoms in Crystalline $Me_2Si[\eta^5\text{-}C_5H_4Fe(CO)]_2$[dppm][a, b]

$Fe'FeP^c$	97.3 (4)	$C_{p_1}SiC_{p_1}{}^c$	109.4 (2)
$Fe'FeC_1{}^c$	49.3 (1)	$C_{p_1}SiC_{m_1}$	108.5 (3)
$Fe'FeC_2{}^c$	48.8 (2)	$C_{p_1}SiC_{m_2}$	109.2 (4)
$Fe'FeC_{p_1}{}^c$	97.6 (1)		
$Fe'FeC_{p_2}{}^c$	119.9 (1)		
$Fe'FeC_{p_3}{}^c$	158.2 (1)		
$Fe'FeC_{p_4}{}^c$	148.4 (1)		
$Fe'FeC_{p_5}{}^c$	111.7 (1)	$FeC_1Fe'{}^c$	81.3 (2)
$Fe'FeC_g{}^{d,d}$	131.0 (–)	FeC_1O_1	138.9 (4)
$PFeC_1$	88.8 (1)	FeC_2O_2	138.6 (4)
$PFeC_2$	87.7 (2)		
$PFeC_{p_1}$	164.3 (1)	$SiC_{p_1}C_{p_2}$	128.4 (3)
$PFeC_{p_2}$	126.7 (1)	$SiC_{p_1}C_{p_5}$	125.5 (3)
$PFeC_{p_3}$	98.5 (1)	$C_{p_2}C_{p_1}C_{p_5}$	105.4 (4)
$PFeC_{p_4}$	102.8 (1)	$C_{p_1}C_{p_2}C_{p_3}$	109.6 (4)
$PFeC_{p_5}$	136.6 (1)	$C_{p_2}C_{p_3}C_{p_4}$	108.3 (4)
$PFeC_g{}^d$	131.7 (–)	$C_{p_3}C_{p_4}C_{p_5}$	107.3 (4)
		$C_{p_4}C_{p_5}C_{p_1}$	109.5 (4)
C_1FeC_2	96.6 (2)		
$C_1FeC_{p_1}$	97.2 (2)	$PC_{11}C_{12}$	121.5 (3)
$C_1FeC_{p_2}$	88.8 (2)	$PC_{11}C_{16}$	119.8 (3)
$C_1FeC_{p_3}$	116.2 (2)	$C_{12}C_{11}C_{16}$	118.7 (4)
$C_1FeC_{p_4}$	153.4 (2)	$C_{11}C_{12}C_{13}$	119.6 (4)
$C_1FeC_{p_5}$	134.5 (2)	$C_{12}C_{13}C_{14}$	121.1 (5)
$C_1FeC_g{}^d$	121.4 (1)	$C_{13}C_{14}C_{15}$	120.0 (5)
$C_2FeC_{p_1}$	105.9 (2)	$C_{14}C_{15}C_{16}$	119.6 (3)
$C_2FeC_{p_2}$	145.4 (2)	$C_{15}C_{16}C_{11}$	120.8 (4)
$C_2FeC_{p_3}$	146.6 (2)	$PC_{21}C_{22}$	123.0 (3)
$C_2FeC_{p_4}$	107.6 (2)	$PC_{21}C_{26}$	119.1 (3)
$C_2FeC_{p_5}$	88.1 (2)	$C_{22}C_{21}C_{26}$	117.9 (4)
C_2FeC_g	120.7 (2)	$C_{21}C_{22}C_{23}$	120.5 (4)
		$C_{22}C_{23}C_{24}$	120.9 (5)
		$C_{23}C_{24}C_{25}$	119.4 (5)
$C_{p_1}FeC_{p_2}$	39.5 (2)	$C_{24}C_{25}C_{26}$	120.3 (5)
$C_{p_1}FeC_{p_5}$	39.1 (2)	$C_{25}C_{26}C_{21}$	121.0 (5)
$C_{p_2}FeC_{p_3}$	38.4 (2)		
$C_{p_3}FeC_{p_4}$	39.1 (2)	$FePC_{11}$	119.2 (1)
$C_{p_4}FeC_{p_5}$	38.8 (2)	$FePC_{21}$	117.1 (1)
		$FePC_b$	110.1 (2)
$C_{p_1}FeC_{p_3}$	65.8 (2)	$C_{11}PC_{21}$	102.9 (2)
$C_{p_1}FeC_{p_4}$	66.0 (2)	$C_{11}PC_b$	103.1 (2)
$C_{p_2}FeC_{p_4}$	65.0 (2)	$C_{21}PC_b$	102.3 (2)
$C_{p_2}FeC_{p_5}$	64.8 (2)		
$C_{p_3}FeC_{p_5}$	64.9 (2)	$PC_bP'{}^c$	111.5 (3)

[a] The numbers in parentheses are the estimated standard deviations in the last significant digit. [b] Atoms are labeled in agreement with Figure 3. [c] Primed (') atoms are related to nonprimed atoms by the crystallographic mirror plane at $y = 1/4$. [d] The symbol C_g is used to denote the center of gravity for the 5-membered ring whose atoms carry a subscripted p.

Table XIII. Bond Angles (deg) Involving Non-Hydrogen and Nongroup Atoms in Crystalline $Me_2Si[\eta^5\text{-}C_5H_4Fe(CO)]_2$[dppp][a, b]

$Fe^bFe^aP^a$	109.6 (6)	$Fe^aFe^bP^b$	108.0 (6)
$Fe^bFe^aC_1$	48.4 (6)	$Fe^aFe^bC_1$	48.7 (6)
$Fe^bFe^aC_2$	49.2 (6)	$Fe^aFe^bC_2$	48.4 (6)
$Fe^bFe^aC_{p_1}{}^a$	95.2 (6)	$Fe^aFe^bC_{p_1}{}^b$	96.2 (6)
$Fe^bFe^aC_{p_2}{}^a$	121.6 (7)	$Fe^aFe^bC_{p_2}{}^b$	124.0 (7)
$Fe^bFe^aC_{p_3}{}^a$	159.6 (8)	$Fe^aFe^bC_{p_3}{}^b$	161.1 (8)
$Fe^bFe^aC_{p_4}{}^a$	140.7 (7)	$Fe^aFe^bC_{p_4}{}^b$	138.3 (7)
$Fe^bFe^aC_{p_5}{}^a$	105.2 (7)	$Fe^aFe^bC_{p_5}{}^b$	104.4 (6)
$Fe^bFe^aC_g{}^{a\,c}$	129.0 (–)	$Fe^aFe^bC_g{}^{b\,c}$	129.1 (–)
$P^aFe^aC_1$	88.4 (7)	$P^bFe^bC_1$	96.6 (7)
$P^aFe^aC_2$	98.9 (7)	$P^bFe^bC_2$	88.7 (6)
$P^aFe^aC_{p_1}{}^a$	154.9 (7)	$P^bFe^bC_{p_1}{}^b$	151.2 (7)
$P^aFe^aC_{p_2}{}^a$	118.6 (7)	$P^bFe^bC_{p_2}{}^b$	112.7 (7)
$P^aFe^aC_{p_3}{}^a$	88.9 (7)	$P^bFe^bC_{p_3}{}^b$	89.3 (7)
$P^aFe^aC_{p_4}{}^a$	95.3 (7)	$P^bFe^bC_{p_4}{}^b$	103.0 (7)
$P^aFe^aC_{p_5}{}^a$	131.3 (7)	$P^bFe^bC_{p_5}{}^b$	140.3 (7)
$C_1Fe^aC_2$	94.3 (7)	$C_1Fe^bC_2$	93.8 (7)
$C_1Fe^aC_{p_1}{}^a$	112.2 (7)	$C_1Fe^bC_{p_1}{}^b$	111.3 (7)
$C_1Fe^aC_{p_2}{}^a$	151.3 (8)	$C_1Fe^bC_{p_2}{}^b$	149.3 (8)
$C_1Fe^aC_{p_3}{}^a$	144.3 (8)	$C_1Fe^bC_{p_3}{}^b$	139.0 (8)
$C_1Fe^aC_{p_4}{}^a$	104.9 (7)	$C_1Fe^bC_{p_4}{}^b$	101.3 (7)
$C_1Fe^aC_{p_5}{}^a$	90.1 (7)	$C_1Fe^bC_{p_5}{}^b$	88.0 (7)
$C_1Fe^aC_g{}^{a\,c}$	124.5 (–)	$C_1Fe^bC_g{}^{b\,c}$	121.1 (–)
$C_2Fe^aC_{p_1}{}^a$	93.9 (7)	$C_2Fe^bC_{p_1}{}^b$	96.3 (7)
$C_2Fe^aC_{p_2}{}^a$	91.0 (7)	$C_2Fe^bC_{p_2}{}^b$	95.7 (7)
$C_2Fe^aC_{p_3}{}^a$	121.3 (8)	$C_2Fe^bC_{p_3}{}^b$	127.0 (8)
$C_2Fe^aC_{p_4}{}^a$	156.4 (8)	$C_2Fe^bC_{p_4}{}^b$	159.5 (8)
$C_2Fe^aC_{p_5}{}^a$	129.7 (7)	$C_2Fe^bC_{p_5}{}^b$	130.5 (7)
$C_2Fe^aC_g{}^{a\,c}$	121.7 (–)	$C_2Fe^bC_g{}^{b\,c}$	125.3 (–)
$C_{p_1}{}^aSiC_{p_1}{}^b$	111.5 (6)		
$C_{p_1}{}^aSiC_{m_1}$	109.6 (6)	$C_{p_1}{}^bSiC_{m_1}$	110.5 (6)
$C_{p_1}{}^aSiC_{m_2}$	110.1 (7)	$C_{p_1}{}^bSiC_{m_2}$	109.4 (7)
$Fe^aC_1Fe^b$	82.9 (7)		
$Fe^aC_2Fe^b$	82.4 (6)		
$Fe^aC_1O_1$	137.5 (9)	$Fe^bC_1O_1$	139.1 (9)
$Fe^aC_2O_2$	138.1 (9)	$Fe^bC_2O_2$	138.5 (9)
$SiC_{p_1}{}^aC_{p_2}{}^a$	129.4 (8)	$SiC_{p_1}{}^bC_{p_2}{}^b$	126.3 (8)
$SiC_{p_1}{}^aC_{p_5}{}^a$	124.6 (8)	$SiC_{p_1}{}^bC_{p_5}{}^b$	128.5 (8)
$C_{p_2}{}^aC_{p_1}{}^aC_{p_5}{}^a$	105.6 (8)	$C_{p_2}{}^bC_{p_1}{}^bC_{p_5}{}^b$	104.8 (8)
$C_{p_1}{}^aC_{p_2}{}^aC_{p_3}{}^a$	109.8 (8)	$C_{p_1}{}^bC_{p_2}{}^bC_{p_3}{}^b$	108.7 (8)
$C_{p_2}{}^aC_{p_3}{}^aC_{p_4}{}^a$	107.7 (9)	$C_{p_2}{}^bC_{p_3}{}^bC_{p_4}{}^b$	109.0 (9)
$C_{p_3}{}^aC_{p_4}{}^aC_{p_5}{}^a$	107.5 (8)	$C_{p_3}{}^bC_{p_4}{}^bC_{p_5}{}^b$	106.6 (9)
$C_{p_4}{}^aC_{p_5}{}^aC_{p_1}{}^a$	109.3 (8)	$C_{p_4}{}^bC_{p_5}{}^bC_{p_1}{}^b$	110.9 (8)
$C_{p_1}{}^aFe^aC_{p_2}$	39.2 (6)	$C_{p_1}{}^bFe^bC_{p_2}{}^b$	38.7 (5)
$C_{p_1}{}^aFe^aC_{p_5}$	39.7 (6)	$C_{p_1}{}^bFe^bC_{p_5}{}^b$	39.1 (6)
$C_{p_2}{}^aFe^aC_{p_3}$	38.4 (6)	$C_{p_2}{}^bFe^bC_{p_3}{}^b$	38.5 (6)
$C_{p_3}{}^aFe^aC_{p_4}$	40.0 (6)	$C_{p_3}{}^bFe^bC_{p_4}{}^b$	38.3 (6)

[a] The numbers in parentheses are the estimated standard deviations in the last significant digit. [b] Atoms are labeled in agreement with Figure 4. [c] The symbols $C_g{}^a$ and $C_g{}^b$ are used to denote the center of gravity for the 5-membered rings whose atoms carry subscripted p's.

corded on a Houston 2000 x-y recorder. Thin-layer coulometry is employed to determine the number of electrons transferred for a particular oxidation. Fast scan cyclic voltammograms are obtained by using a Krohn-Hite Model 5200 function generator to provide 1–100 V/s triangular waveforms, and the resultant current–voltage curves are recorded on a Tektronix 5441 storage oscilloscope operating in the x-y amplifier mode. The stored voltammograms are photographed with a Tektronix C-5 oscilloscope camera.

Preparation of $Me_2Si[\eta^5\text{-}C_5H_4Fe(CO)_2]_2$[dppm] (3a). A benzene (250 mL) solution of $Me_2Si[\eta^5\text{-}C_5H_4Fe(CO)_2]_2$ (1; 0.50 g, 1.2 mmol) and dppm (0.50 g, 1.3 mmol) is irradiated for 8 h. The mixture is then filtered and the solvent removed under vacuum. The crude product is dissolved in acetonitrile (15 mL) and set aside at −25 °C for 1 h. The dark green crystals of **3a** that form are collected, washed with CH_3CN (2 × 10 mL), and air dried (0.75 g, 85%): IR spectrum (cm^{-1} in CH_2Cl_2) ν(CO) 1682. Anal. Calcd for $C_{39}H_{36}Fe_2O_2P_2Si$: C, 63.43; H, 4.91. Found: C, 63.29; H, 4.97.

Preparation of $Me_2Si[\eta^5\text{-}C_5H_4Fe(CO)]_2$[dppe] (3b). A benzene (250 mL) solution of **1** (0.50 g, 1.2 mmol) and dppe (1.0 g, 2.6 mmol) is irradiated for ~20 h. The solution is filtered and the solvent removed under vacuum. The crude product is washed with acetone (4 × 25 mL) to remove excess ligand. The green powder that remains is dissolved in C_6H_6–CH_2Cl_2 (~5 mL, 1/1, v/v) and column chromatographed (alumina III, 3 × 30 cm). Elution with benzene produces an initial green band and a second, slower moving blue band. The blue band is collected and the solvent removed and identified as complex **4b** by spectroscopic data. The green band is collected and the solvent removed to give **3b** (0.54 g, 60%) as a green powder: IR spectrum (cm^{-1} in CH_2Cl_2) ν(CO) 1680. Anal. Calcd for $C_{40}H_{38}Fe_2O_2P_2Si$: C, 63.89; H, 5.09. Found: C, 63.94; H, 5.17.

Preparation of $Me_2Si[\eta^5\text{-}C_5H_4Fe(CO)]_2$[dppp] (3c). A benzene (250 mL) solution of **1** (0.50 g, 1.2 mmol) and dppp (1.0 g, 2.5 mmol) is irradiated for ~20 h. The solution is filtered and the solvent removed. The crude product is dissolved in benzene (~4 mL) and placed on a column (alumina III, 3 × 30 cm). Elution with benzene produces two bands, a fast moving green band and a second, slower moving, blue-green band. The green band is collected and the solvent removed to give a green oil. The oil is treated with Et_2O (20 mL) and set aside at −25 °C for several hours. The green solid is collected by filtration to give pure **3c** (~0.58 g, ~64%): IR spectrum (cm^{-1} in CH_2Cl_2) ν(CO) 1680.

Anal. Calcd for $C_{41}H_{40}Fe_2O_2P_2Si$: C, 64.25; H, 5.26. Found: C, 64.43; H, 5.66.

Preparation of $[Me_2Si[(\eta^5\text{-}C_5H_4)_2Fe_2(CO)_3]]_2[PhP(CH_2)_nPPh_2]$ (n = 2 (4b) and n = 3 (4c)). A benzene (~50 mL) solution of 1 (1.00 g, 2.6 mmol) and dppe (0.40 g, 1.1 mmol) is irradiated in a Pyrex schlenk tube (3 × 15 cm) for ~20 h. This mixture is filtered and the solvent removed. The crude product is dissolved in CH_2Cl_2 (~5 mL) and then placed on a column (alumina III, 3 × 30 cm), and elution with benzene gives an initial green band (identified as **3b**), and a second blue-green band. The blue-green band is collected and the solvent removed to give **4b** as a blue-green powder (0.90 g, 71%): IR spectrum (cm^{-1} in CH_2Cl_2) ν(CO) 1937 (s), 1731 (s), 1680 (w). Anal. Calcd for $C_{56}H_{52}Fe_4O_6P_2Si_2$: C, 57.86; H, 4.51. Found: C, 57.75; H, 4.51.

In a similar manner **4c** is prepared and isolated as blue-green crystals (70%). Anal. Calcd for $C_{57}H_{54}Fe_4O_6P_2Si_2{\cdot}C_6H_6$: C, 60.31, H, 4.82. Found: C, 59.94; H, 5.10.

Crystallographic Summary for $Me_2Si[\eta^5\text{-}C_5H_4Fe(CO)]_2$[dppm] (3a). Pertinent crystal and intensity data are listed in Table V. Complete details of the crystallographic analysis are given in Table A (crystallographic report) of the supplementary material. The structure is first solved by direct methods, the 25 non-hydrogen atoms are located on an E map calculated from a trail set of phases. The hydrogen atoms are located by difference Fourier techniques or are placed in their calculated positions and then refined. All non-hydrogen atoms are refined anisotropically, and the hydrogens are refined by using isotropic thermal parameters to give final values of $R_1 = 0.041$ and $R_2 = 0.045$ where $R_1 = \sum||F_o| - |F_c||/\sum|F_o|$ and $R_2 = [\sum w(|F_o| - |F_c|)^2/\sum|F_o|^2]^{1/2}$. Listings of final positional parameters for non-hydrogen and hydrogen atoms are given in Tables VI and VIII, respectively. Thermal parameters for non-hydrogen atoms are set out in Table C, and the observed and calculated structure factors are presented in Table E of the supplementary material.

Crystallographic Summary for $Me_2Si[\eta^5\text{-}C_5H_4Fe(CO)]_2$[dppp] (3c). Pertinent crystal and intensity data are listed in Table V. Complete details of the crystallographic analysis are given in Table B (crystallographic report) of the supplementary material. The structure is initially solved for the four heaviest atoms (Fe, P) by direct methods, and the remaining non-hydrogen atoms are located by difference Fourier techniques. The selected hydrogen atoms are placed in their calculated positions (assuming idealized sp^2 and sp^3 hybridization) and are refined as contributions of constant position and thermal (B = 4.0 Å^2) parameters. All non-hydrogen and nongroup atoms are refined anisotropically, and the group atoms (four phenyl rings) are refined by using isotropic thermal parameters to give final values of $R_1 = 0.067$ and $R_2 = 0.076$. Listings of final positional parameters for non-hydrogen and nongroup atoms and group atoms are given in Tables VII and IX, respectively. Thermal parameters for non-hydrogen and nongroup atoms are presented in Table D, and the observed and calculated structure factors are given in Table F of the supplementary material.

Complex **3c** is found to crystalize with solvent in a 1:1 ratio. The solvent however is a mixture of CH_2Cl_2 and CH_3NO_2 and is observed as a somewhat random ratio of the two solvents. In addition to what appears to be a random incorporation of CH_2Cl_2 and CH_3NO_2 into the crystal lattice there is also disordering of the solvent molecules. As a result of these conditions six of the largest peaks in the Fourier difference map have been assigned to solvent atoms and refined with anisotropic thermal parameters.

Acknowledgment. G.O.N. gratefully acknowledges partial support of this research by the Research Corp., the Camille and Henery Dreyfus Foundation, and the donors of the Petroleum Research Fund, administered by the American Chemical Society. G.O.N. also thanks the NSF (Grant CHE-8102918) for funds obtained. N.R.A. acknowledges the NSF (Grant CHE-8017571) for support of this work.

Registry No. 1, 42830-83-1; **3a**, 78373-20-3; **3b**, 78357-02-5; **3c**, 87174-20-7; **4b**, 78357-01-4; **4c**, 87156-99-8; $[C_5H_5Fe(CO)]_2$[dppe], 12701-59-6; $[C_5H_5Fe(CO)]_2$[dppm], 60508-02-3.

Supplementary Material Available: Crystal structure analysis reports (Table A, **3a**; Table B, **3c**) and tables of anisotropic thermal parameters (Table C, **3a**; Table D, **3c**) and bond lengths and angles involving hydrogen atoms in **3a** (Table E) and listings of structure factors for **3a** and **3c** (44 pages). Ordering information is given on any current masthead page.

(13) G.O.N. is presently located at Tennessee Eastman Co., Research Laboratories, Kingsport, TN 37662.